

# A Re-Learning Based Post-Processing Step For Brain Tumor Segmentation From Multi-Sequence Images

**Naouel Boughattas**

*LR-SITI*

*University of Tunis El Manar*

*ROMMANA 1068, Tunis-B.P. n°94, Tunisia*

*and*

*LITIS-Quantif*

*University of Rouen*

*22 boulevard Gambetta 76183 Rouen, France*

*naouel.boughattas@gmail.com*

**Maxime Berar**

*LITIS-Quantif*

*University of Rouen*

*22 boulevard Gambetta 76183 Rouen, France*

*maxime.berar@univ-rouen.fr*

**Kamel Hamrouni**

*LR-SITI*

*University of Tunis El Manar*

*ROMMANA 1068, Tunis-B.P. n°94, Tunisia*

*kamel.hamrouni@enit.rnu.tn*

**Su Ruan**

*LITIS-Quantif*

*University of Rouen*

*22 boulevard Gambetta 76183 Rouen, France*

*su.ruan@univ-rouen.fr*

---

## Abstract

We propose a brain tumor segmentation method from multi-spectral MRI images. The method is based on classification and uses Multiple Kernel Learning (MKL) which jointly selects one or more kernels associated to each feature and trains SVM (Support Vector Machine).

First, a large set of features based on wavelet decomposition is computed on a small number of voxels for all types of images. The most significant features from the feature base are then selected and a classifier is then learned. The images are segmented using the trained classifier on the selected features. In our framework, a second step called re-learning is added. It consists in training again a classifier from a reduced part of the training set located around the segmented tumor in the first step. A fusion of both segmentation procures the final results.

Our algorithm was tested on the real data provided by the challenge of Brats 2012. This dataset includes 20 high-grade glioma patients and 10 low-grade glioma patients. For each patient, T1, T2, FLAIR, and post-Gadolinium T1 MR images are available. The results show good performances of our method.

**Keywords:** Cerebral MRI, Tumor, Segmentation, Feature Selection, Multiclass, Classification, Multiple Kernel Learning, Multimodal.

---

## 1. INTRODUCTION

Brain tumor is among the most frequent cancers and its mortality rate is very high. The most aggressive forms of the disease, classified as HG gliomas (High-Grade gliomas), possess a two years survival mean rate and even less than two years and require an immediate treatment. The

disease variants having a slow development, classified as LG gliomas (Low-Grade gliomas), have a many years' life expectancy. For these two types of gliomas, various protocols of medical imaging are necessary before and after the treatment to estimate the progress of the disease as well as the performance of the chosen treatment strategy. As it provides a good soft tissue contrast, Magnetic Resonance Imaging (MRI) is currently the standard technique for brain tumor diagnostic [1, 2, 3]. MRI can also produce different types of tissue contrasts by varying excitation and repetition times, enhancing different aspects of the tissues and revealing different subregions of the tumor such as necrotic, active or edema subregions. Despite continuous advances in imagery technology, brain tumors, owing to their extremely heterogeneous shapes, appearances and locations still present a serious challenge to segmentation techniques.

In the literature, a large number of medical image segmentation methods were proposed. Among these methods, the methods based on classification are particularly well adapted for multi-sequence data: We can merge multi-sequence data by selecting features. In the case of supervised learning, classification methods are based on two main elements: the first element is the description of the data, in a features extraction step, aiming to represent in a discriminative way the raw information given by voxels intensity observed through several modalities. The second element is the learning of a decision rule from labelled data.

In our segmentation problem, the most discriminative features are unknown a priori. Besides, they are different according to the modality. Thus it is necessary to select them among all the features extracted from the images multi-sequence. Over the years, many features were proposed in the literature, trying to include a lot of information or to supply a high distinctive power. From our point of view, to obtain a good classification, the choice of the features is important, particularly in the case of several types of image such as the MRI sequences. However, we do not know a priori the most informative features for each type of MRI sequence. Thus, it is necessary to extract various types of feature and choose the most significant ones for each MRI sequence before the classification, according to their individual discrimination power [4], or according to their class separability [5].

Multiple Kernel Learning (MKL) [6] jointly operates kernel selection and classification via a SVM [10]. Its principle is to associate one or more kernels to each feature. The MKL algorithm will then jointly determine the weight associated with each kernel (feature selection) and the separating hyperplans of an SVM (classification step). A sparse constraint is also applied on the kernel weights in order to select as few features as needed. Regarding the advantages of this technique, MKL is adopted in our brain tumor segmentation framework.

In this paper, we propose a semi-automatic brain tumor segmentation method from MRI multi-sequence. The proposed method is based on classification and uses a MKL algorithm to exploit the diversity and the complementarity of the data supplied by the different images. The method needs a minimal human interaction to include doctor's expertise and produces relatively precise results. First, a large set of features based on wavelet coefficients is computed on all types of images from a small number of voxels, allowing us to build a training feature base. Using the MKL algorithm, we can associate one or more kernels to each feature in order to solve jointly the two problems: (1) selection of the features and their corresponding kernels, (2) training of the classifier. The tumor and edema are then segmented using the trained classifier on the selected features extracted from the whole image volumes. Finally, a post-processing step is performed to improve the results by using a second learning step (second application of the MKL algorithm). Combining the two tumor regions obtained from the first and the second learnings gives the final results.

The idea of using the MKL-SVM algorithm to segment brain tumor from multi-spectral MRI images was published in previous work [12]. In this paper we add a post-processing step based on a re-learning step.

We have tested our method using the database provided by the Multimodal Brain Tumor Segmentation (BraTS) 2012 challenge [11]. It is a large dataset of brain tumor MR scans in which the tumor and edema regions have been manually delineated and been made available to the public.

The paper is organized as follows: The next section of this paper is devoted to our method and its different steps, including a brief presentation of the MKL. Then, we compare our results in the different steps of the method. We conclude finally.

## 2. METHOD

As seen Figure1, our proposed methods is divided into three main steps : a learning step, a classification step and a post processing step.

The purpose of the learning step is to solve the MKL-SVM problem and to validate its regularization parameter  $C$ , based on a reduced set of labelled voxels extracted from a MRI sequence. This step itself, is based on three stages : the labeling of a reduced set of voxels, the computing of the features associated with these voxels and the MKL-SVM training.

The MKL-SVM training is repeated several times to select the regularization parameter  $C$  associated to the MKL-SVM problem : First, the features are extracted from a reduced set of voxels labelled by experts. Then, the most relevant features among all the features are selected by the MKL method using a sparsity constraint (to reduce the number of features). The hyperparameter  $C$  of the MKL algorithm is estimated during this learning step.

The classification step is a two stages procedure: first, we calculate the features associated to all the voxels of all MRI images. Then, we use the MKL-SVM classifier using the already chosen value of  $C$ , to segment three classes: edema, tumor and healthy tissues.

The post-processing step is used to correct some errors in the tumor boundary and the edema boundary. It is based on a re-learning step on a reduced area around the first detected tumor and edema areas. Very small regions are filtered for both learnings. The final result is obtained by merging the results of both learnings and by applying a 3D connection on the fusion result.

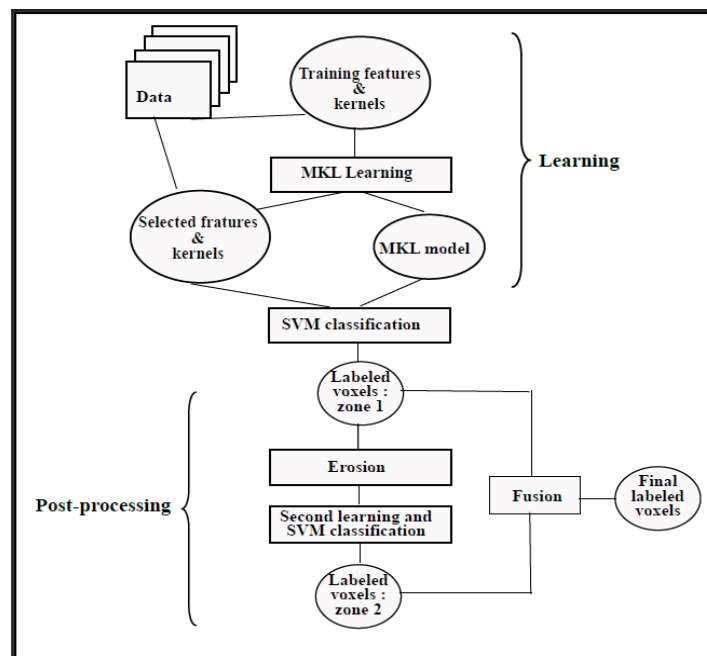


**FIGURE 1:** Proposed Framework of Our Method.

### 2.1 Learning Step

The learning step takes place in three stages: the labeling of a reduced set of voxels, the computing of the associated features and the MKL-SVM training. This last stage allows to validate and to select the regularization parameter C associated to the MKL-SVM problem.

#### 3.2.1 Training Set

For each patient, the expert is brought to select points on the border of the tumor, the border of the edema as well as on a healthy zone, on a single slice in a single sequence. These points allow to draw the boundaries of each tissue. From these boundaries, we can generate a learning set for each tissue class. Numerous features can be extracted to describe brain tumor texture in MR images, such as intensity based features [7], texture based features [8] and wavelet coefficients [7].

#### 3.2.2 MKL Training

We can associate one or more kernel functions to each type of features for each image sequence. Each kernel is associated with a positive coefficient reflecting the importance of the corresponding feature in the classification. As a linear combination of these kernels weighted with these coefficients is also a kernel, a SVM with this new kernel could be used to classify. The best classification is obtained when the best combination of the kernels is found.

Multiple kernel learning methods were introduced by Lanckriet et al. in [6] and have been developed to determine the positive weight  $d_m$  associated to each kernel  $k_m$ . In a MKL-SVM framework, the decision function has the following form :

$$f(x) = \sum_{i=1}^l \sum_{m=1}^p \alpha_i d_m k_m(x^m, x_i^m)$$

where the  $\alpha_i$  are the weights associated to each training example  $x_i$  of label  $y_i$  and  $x_i^m$  and  $x^m$  represents the feature associated to kernel  $k_m$ . If  $f(x) > 0$ , the corresponding point is associated to class 1, otherwise class 0.

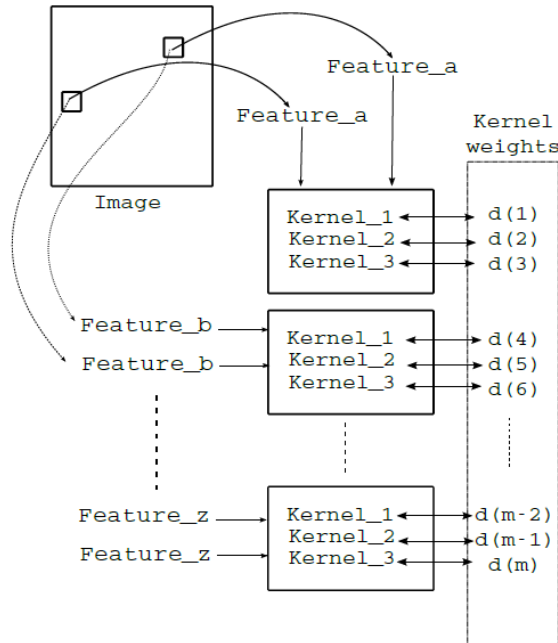


FIGURE 2: Feature and Kernel Selection via Kernel Weights.

As seen in Figure 2, we can associate each kernel weight to a single kernel applied to one feature. The sparsity constraint on the kernel weights allows us to select both the informative features and adapted kernels. In practice, we can use several kernels of the same family with different parametrizations.

Numerous methods and formulations exist for solving the MKL problem in literature. We chose the SimpleMKL algorithm [9] in our method mainly because a version is provided for multi-class settings using a common kernel weights determination for all classes. It will enable a better interpretation of the selected kernels. The SimpleMKL algorithm is based on solving the primal problem using a simple gradient method. The primal problem determines jointly the kernel functions  $f_m$ , the kernel weights  $d_m$  and the soft margin parameters  $\xi_i$  :

$$\begin{aligned} \min_{\{f\}_m, \xi, d} \quad & \frac{1}{2} \sum_m d_m \|f_m\|_{\mathbb{H}_n} + C \sum_i \xi_i \\ \text{s.t.} \quad & y_i \sum_m f_m(x_i) \geq 1 - \xi_i, \quad \xi_i \geq 0, \quad \forall i, \\ & \sum_m d_m = 1, \quad d_m \geq 0, \quad \forall m. \end{aligned}$$

The  $l_1$ -norm sparsity constraint on the positive weights  $d_m$  is given by fixing their sum equal to one. The regularisation hyperparameter C is initialized with a very small value and then incremented regularly. On a multi-class problem, there is still an interval of C-value where the segmented region is stable, corresponding to stable kernel weights. The adopted validation strategy is then : once the variations of kernel weights become lower than a given threshold ( $\xi_i$ ), the current value of C is chosen.

## 2.2 MKL based SVM Classification

Thanks to the learning step and the the sparse constraint, we can use only the subset of features associated to the chosen kernels (with non-null weights  $d_m$ ) to classify the voxels. Indeed, the values of  $d_m$  define if the corresponding features are selected. If  $d_m = 0$ , the corresponding feature is not selected. Test features are then computed for all the voxels of the different MRI volumes, and the MKL-SVM algorithm is run using the  $C_{stab}$  value and the learned MKL model.

## 2.3 Post-processing Step and Re-learning

The aim of the post-processing step is to improve the obtained classification results. Very small regions are first eliminated by using morphological operations. A re-learning step is then performed, which can be viewed as a reapplication of our MKL-SVM algorithm on a reduced area including abnormal tissues and normal tissues around the tumor area (a second learning step, a second feature extraction step and a second classification step). This second learning allows to train the classifier specifically to deal with boundary regions. New results of tumor and edema segmentations are finally obtained. the second learning improves tumor detection for the most of the patients. For that reason, we combine the new results with the first step ones in order to find the best segmentation using two simple fusion rules : the union of the two sets of tumor labelled voxels for tumor segmentation and the set of edema labelled voxels of the first trial for edema segmentation. A 3D connection is finally applied to eliminate isolated voxels. The fusion strategy is presented in Table 1: 1 is the edema label, 2 is the tumor label and 0 is the healthy tissue label. The post-processing step is presented in Figure 3.

<b>Fusion</b>	<b>0</b>	<b>1</b>	<b>2</b>
<b>0</b>	0	0	2
<b>1</b>	1	1	2
<b>2</b>	2	2	2

**TABLE 1:** The fusion strategy. Bold column : first learning labels. Bold line: second learning labels.

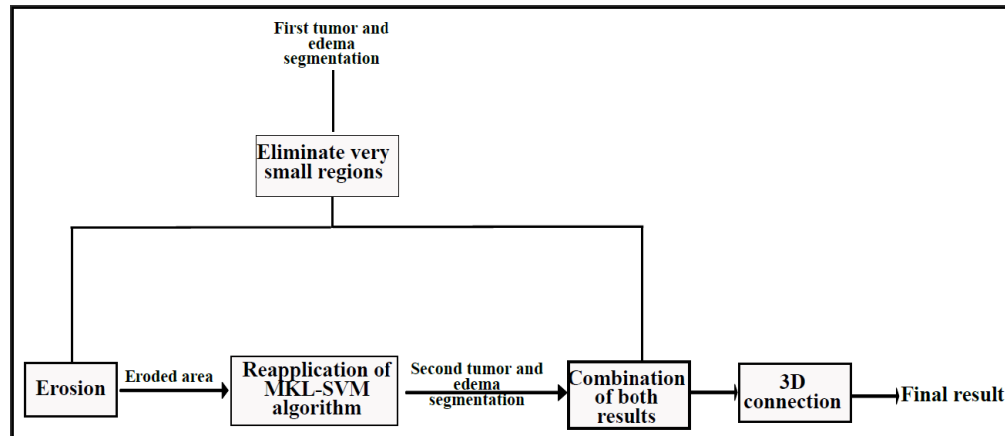


**FIGURE 3:** The Post-processing Step.

### 3. MATERIAL AND RESULTS

#### 3.1 Material

We evaluate our approach on real patients MRI of the dataset of the MICCAI 2012 BraTS challenge. This dataset includes 20 high-grade glioma patients, where tumor tissues and healthy tissues are well differentiated, and 10 low-grade glioma patients, where tumor tissues and healthy tissues are poorly differentiated, both with and without resection, along with expert annotations for active tumor and edema. For each patient, T1, T2, FLAIR, and post-Gadolinium T1 MR images are available as seen in Figure 4. All volumes were linearly co-registered to the T1 contrast images, skull stripped, and interpolated to 1mm isotropic resolution. The MR scans are provided as well as the corresponding reference segmentations.

Figure 5 shows examples of slices and their corresponding ground truths for four patients: two from the HG dataset and two others from the LG dataset.

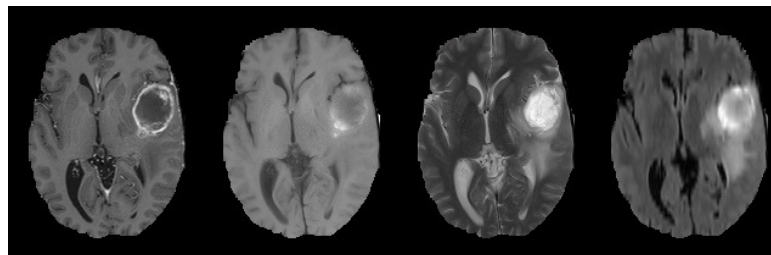


**FIGURE 4:** Slices of the four volumes of a patient (from left to right: post-Gadolinium T1, T1-weighted, T2-weighted and Flair).

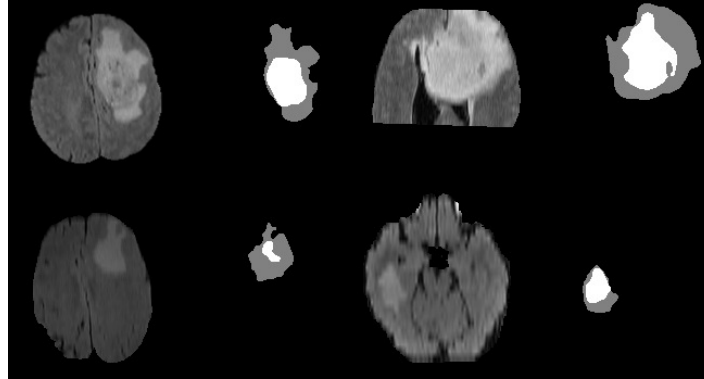


**FIGURE 5:** Example slices and their ground truths for 4 patients. left column : patient HG11 (top) patient HG14 (bottom) right column : patient LG02 (top) patient LG14 (bottom).

### 3.2 Experiments & Results

In this paper, we used a set of features based on Multilevel 2-D Discrete wavelet decomposition calculated on a patch surrounding each labeled voxel, as feature for brain tumor description in MR images [7]. The whole feature set is composed of nine different details and one residual coefficients of Haar 2D wavelet decomposition calculated separately on each modality, combined through Gaussian kernels with different parameters defined as the standard deviation of the feature multiplied by factors 0:1, 1 or 10. It results on 120 kernels.

Given a fixed value of the regularisation parameter  $C$ , we studied the influence of the size of the learning set to the Dice score value and to the learning time. The Dice score as well as the learning time increase with the increasing of the learning set. With the best value of dice score and a reasonable learning time, the chosen size of the learning set is 150 points.

As presented earlier in this paper, we do a 're-learning' step and merge the labels in a late fusion step. So for each patient, we can provide three evaluation results corresponding to the segmentations obtained by the initial learning, by the second learning and by the fusion of the labels. That allows to show improvements given by the re-learning and fusion steps. We will also present as a control experiment the dice score of the segmentation given by the most-weighted kernel of the MKL. Ideally, all three evaluations results should perform better than any single kernel of the MKL kernel set. The dice score is computed using the on-line tool available during the challenge.

#### 3.2.1 Results for High-Glioma Patients

Table 2 details the Dice scores for the high-grade patients of the dataset. We compare results of the different steps of the method as well as the results given by the single best kernel. It can be observed that the results using the best single kernel in the control experiment are worse than the results obtained at each step of the method, except for patient HG14. In this case, the results of the two-first steps and the control experiment are similar, but the fusion significantly improve the results. That means a fusion of the different steps allows to improve the results.

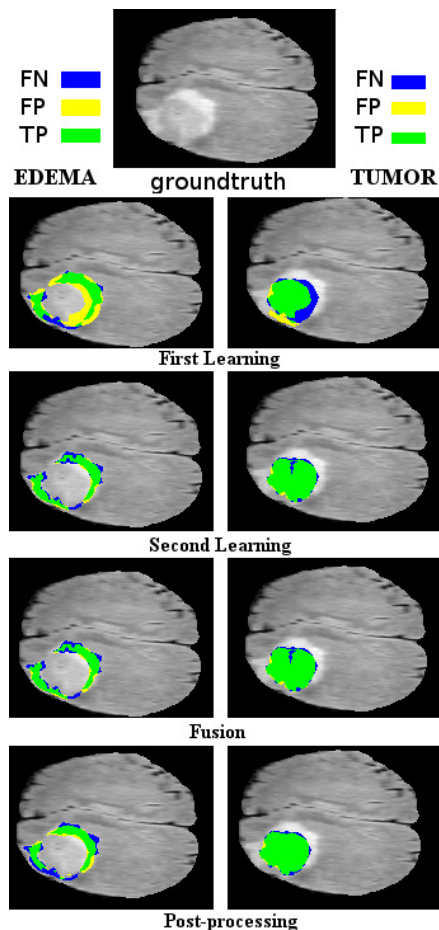
The edema mean dice score of the second learning step segmentation is lower than that of the first segmentation. However the tumor mean dice score lightly increases. That shows that the fusion strategy of the two different classification results enables a better segmentation of the core part of the tumor, with a 5% higher mean dice score for this class. It proves a good performance of our choice of fusion strategy of the two segmentation steps. Figure 6 shows a first example of segmentation results for one high gliomas patients (HG14) detailed at each step of our method. The initial segmentation is first improved by the second learning and further refined by the fusion strategy and post-processing step (3D connection). However, as seen in Figure 7, the second learning can lead to some false positives for edema labelling, but this can be corrected by the fusion strategy. This is reflected in the corresponding mean dice score.

Volume	1rst training		2nd training		Fusion		Best kernel	
	E	T	E	T	E	T	E	T
HG01	0.62	0.60	0.60	0.66	0.64	0.67	0.60	0.46
HG02	0.74	0.51	0.58	0.61	0.70	0.61	0.52	0.34
HG03	0.82	0.84	0.81	0.76	0.80	0.77	0.39	0.74
HG04	0.52	0.69	0.51	0.80	0.51	0.80	0.46	0.54
HG05	0.47	0.33	0.48	0.39	0.44	0.36	0.08	0.20
HG06	0.45	0.59	0.53	0.56	0.48	0.57	0.34	0.52
HG07	0.53	0.60	0.46	0.67	0.55	0.70	0.50	0.44
HG08	0.71	0.68	0.76	0.84	0.72	0.85	0.27	0.51
HG09	0.68	0.71	0.60	0.59	0.69	0.74	0.63	0.59
HG10	0.39	0.59	0.23	0.49	0.48	0.54	0.29	0.08
HG11	0.77	0.87	0.45	0.73	0.75	0.87	0.45	0.68
HG12	0.42	0.61	0.48	0.37	0.45	0.64	0.27	0.10
HG13	0.59	0.70	0.56	0.66	0.56	0.72	0.47	0.68
HG14	0.24	0.52	0.23	0.67	0.29	0.75	0.28	0.58
HG15	0.78	0.87	0.70	0.87	0.77	0.87	0.34	0.78
HG22	0.66	0.41	0.52	0.61	0.65	0.63	0.65	0.17
HG24	0.62	0.71	0.52	0.75	0.61	0.76	0.38	0.19
HG25	0.51	0.55	0.51	0.32	0.41	0.35	0.08	0.20
HG26	0.71	0.50	0.54	0.46	0.70	0.53	0.41	0.14
HG27	0.67	0.80	0.56	0.77	0.67	0.81	0.55	0.55
<b>Mean</b>	0.60	0.63	0.54	0.64	0.60	0.68	0.40	0.42
<b>Min</b>	0.24	0.33	0.23	0.32	0.29	0.35	0.08	0.08
<b>Max</b>	0.82	0.87	0.81	0.87	0.80	0.87	0.65	0.78

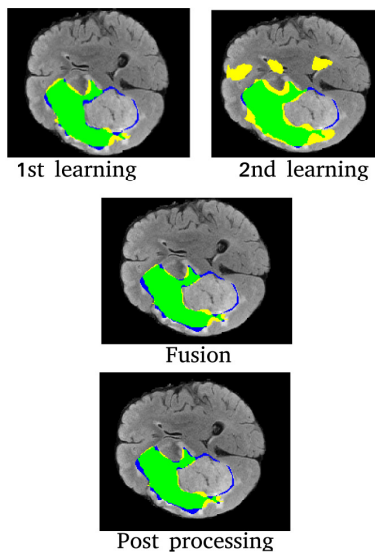
**TABLE 2:** Detailed MKL-SVM segmentation results of high-grade gliomas patients in the BRATS dataset. Dice score is reported for the segmentation of edema (E) and active tumor (T).

Table 3 shows the mean weights of the 120 initial kernels with respect to the different modalities and wavelet coefficients (Horizontal, Vertical, Diagonal, Accuracy) at each decomposition levels (N). Each table cell contains the three kernel weights represented in percentages associated to a single feature through three different Gaussian kernel. The selected kernels correspond to non-null weights. Some of them are selected with very small weights lower than 1%, which are denoted by  $\epsilon$  in the table. Note that only 40 mean kernel weights are non-null. In fact, only an average of 8 features is selected per patient, which means that the segmentation step only requires the computation of a very small number of features among all 120 features on the whole image volumes.

The most-weighted kernels correspond to the details of the last level of the wavelet decomposition (table 2, N=3, A). This information is complemented by kernels with very small weights ( $\epsilon$ ) which are selected at all level of decomposition. Even with very small weights, these kernels contribute to the decision. Thanks to the sparsity constraint, uninformative kernels won't be selected. Through the selected kernels, all modalities take part in the classification process. Flair and T2 modalities have the three most weighted kernels. Their weights have about the same order of magnitude. These modalities are known to be decisive in the segmentation process and are retrieved by our kernel selection method. Moreover, we can see that the other modalities especially T1c can also contribute to the segmentation process depending on patient.



**FIGURE 6:** Examples of intermediary segmentations for one slide of Patient HG0014. Left: edema region, Right: tumor region Green : True Positives, Blue : False Negatives and Yellow : False Positives.



**FIGURE 7:** Segmentation results for Patient HG0027 for the Edema region. Green : True Positives, Blue : False Negatives and Yellow : False Positives.

wavelet coefficients	Modality			
	T1	T1c	T2	Flair
N=1, H	0/0/0	$\mathcal{E} / \mathcal{E} / 0$	0/0/0	0/0/0
N=1, V	0/0/0	$\mathcal{E} / \mathcal{E} / 0$	0/ $\mathcal{E} / 0$	0/0/0
N=1, D	0/0/0	0/0/0	0/ $\mathcal{E} / 0$	0/0/0
N=2, H	$\mathcal{E} / 0 / 0$	$\mathcal{E} / \mathcal{E} / 0$	0/0/0	0/1/0
N=2, V	$\mathcal{E} / 0 / 0$	$\mathcal{E} / \mathcal{E} / 0$	0/ $\mathcal{E} / 0$	0/ $\mathcal{E} / 0$
N=2, D	0/0/0	$\mathcal{E} / \mathcal{E} / 0$	0/ $\mathcal{E} / 0$	0/0/0
N=3, A	$\mathcal{E} / 11 / 0$	2/5/8	0/2/16	0/20/21
N=3, H	0/0/0	$\mathcal{E} / \mathcal{E} / 0$	0/1/0	0/2/0
N=3, V	$\mathcal{E} / \mathcal{E} / 0$	$\mathcal{E} / \mathcal{E} / 0$	0/ $\mathcal{E} / 0$	0/3/0
N=3, D	0/0/0	$\mathcal{E} / \mathcal{E} / 0$	0/ $\mathcal{E} / 0$	0/0/0

**TABLE 3:** Detailed Kernel weights (%) of the three gaussian kernel associated to each feature (HG patients).  $\mathcal{E}$  denotes selected kernels with very small associated weights.

### 3.2.2 Results for Low-Glioma Patients

Table 4 details the Dice scores for the low-grade patients of the dataset obtained at each step of the method as well as the results given by the single best kernel control experiment. The first learning step is not as effective as the control experiment for three patients out of 10. However in one of those cases (LG12), the fusion strategy with the second set allows to compensate the errors. These results are less globally satisfying than the results for High-grade patients, because the quality of images is not as good as for high grade patients. Notice that if the fusion and re-learning steps appear inefficient on average compared to the segmentation results of the first learning, they compensate bad first learning step results as indicated by the major amelioration on the tumor dice score.

Table 5 shows the mean weights of selected kernels among the 120 initial kernels with respect to the different modalities and wavelet decomposition levels. The selection pattern among the different features and modalities is quite similar to the high-gliomas case, except for the weight given for the most-weighted kernel and the reduction of the number of complementary kernels. This concentration of the weight on one kernel explains why the control experiment performs more similarly than our methods in LG patient case. Figure 8 shows an example of our segmentation results on a low glioma patients (LG12) at different steps of the method. As we can see, the post-processing step improves significantly tumor and edema detection.

Volume	1rst training		2nd training		Fusion		Best kernel	
	E	T	E	T	E	T	E	T
LG01	0.29	0.26	0.24	0.51	0.27	0.52	0.28	0.36
LG02	0.71	0.73	0.61	0.58	0.61	0.58	0.71	0.69
LG04	0.60	0.64	0.53	0.56	0.57	0.55	0.42	0.26
LG06	0.67	0.54	0.65	0.41	0.67	0.42	0.24	0.52
LG08	0.58	0.69	0.51	0.56	0.58	0.69	0.59	0.44
LG11	0.41	0.86	0.39	0.87	0.39	0.87	0.44	0.85
LG12	0.51	0.66	0.42	0.80	0.55	0.80	0.53	0.70
LG13	0.43	0.69	0.26	0.57	0.45	0.61	0.13	0.32
LG14	0.15	0.46	0.17	0.50	0.18	0.50	0.15	0.52
LG15	0.60	0.78	0.54	0.77	0.58	0.77	0.15	0.73
<b>mean</b>	0.49	0.63	0.43	0.61	0.49	0.63	0.36	0.54
<b>min</b>	0.15	0.26	0.17	0.41	0.18	0.42	0.13	0.26
<b>max</b>	0.71	0.78	0.65	0.87	0.67	0.87	0.71	0.85

**TABLE 4:** Detailed MKL-SVM segmentation results of low-grade gliomas patients in the BRATS dataset. Dice score is reported for the segmentation of the edema and the active tumor.

wavelet coefficients	modality			
	T1	T1c	T2	Flair
N=1, H	0/0/0	0/0/0	0/0/0	0/0/0
N=1, V	0/0/0	$\mathcal{E}$ /0/0	0/0/0	0/0/0
N=1, D	0/0/0	0/0/0	0/0/0	0/0/0
N=2, H	$\mathcal{E}$ /0/0	$\mathcal{E}$ /0/0	0/ $\mathcal{E}$ /0	0/0/0
N=2, V	$\mathcal{E}$ /0/0	$\mathcal{E}$ /0/0	0/0/0	0/0/0
N=2, D	0/0/0	0/0/0	0/0/0	0/0/0
N=3, A	4/8/0	3/3/ $\mathcal{E}$	0/ $\mathcal{E}$ /17	0/45/9
N=3, H	$\mathcal{E}$ /0/0	$\mathcal{E}$ / $\mathcal{E}$ /0	0/2/0	0/ $\mathcal{E}$ /0
N=3, V	2/ $\mathcal{E}$ /0	$\mathcal{E}$ /0/0	0/1/0	0/1/0
N=3, D	$\mathcal{E}$ /0/0	0/ $\mathcal{E}$ /0	0/ $\mathcal{E}$ /0	0/0/0

**TABLE 5:** Kernel weights (%) of the three gaussian kernel associated to each feature (LG patients).  $\mathcal{E}$  denotes selected kernels with very small associated weights.

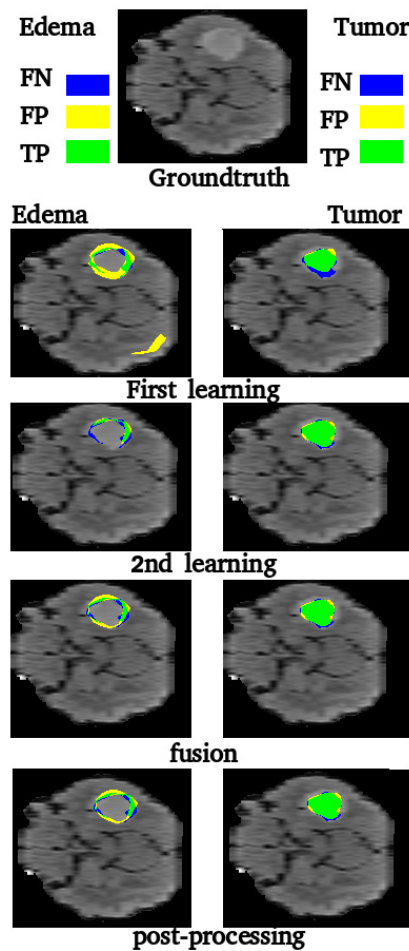


**FIGURE 8:** Examples of intermediary segmentations for one slide of Patient LG0014 without (top) and with (bottom) the post processing step. The left column : edema region, The right column : tumor region Green : True Positives, Blue : False Negatives and Yellow : False Positives.

### 3.2.3 Discussion

In order to evaluate the performance of the proposed method, we use the mean Dice scores to compare our segmentation results with those of participating methods of the challenge BRATS'12. This comparison is shown in Table 6. The winning methods of the challenge were : Zikic et al. [13], Bauer et al. [10] and Hamamci et al. [14]. Only Hamamci et al. don't use classification based on features extracted from all modalities. Compared with these three methods, only the method of Zikic et al. [13] performs better than ours. Among all the other methods of the challenge, only that of Subbana et al. [11] performs slightly better than us. The methods presented by Zikic et al. [13] and Geremia et al. [15] use forest classification. The method of Bauer et al. [10] replaced a SVM judged less sophisticated used in a previous version of their method by a random forest classification. In [11], Subbanna et al. used a Bayesian classifier. However, for all those methods the classification step is either completed by a priori information learned on other patients such as tissue-specific intensity based models [13] or regularized via a Conditional Random Field [10], while our method uses a very simple training process.

From Table 6, we can see that our method globally performs better in both edema and tumor segmentation for low-grade dataset than all methods of the challenge, but less for the high-grade dataset.

	HG		LG		global
	Edema	Tumor	Edema	Tumor	
<b>MKL-SVM</b>	<b>0.60</b>	<b>0.68</b>	<b>0.49</b>	<b>0.63</b>	<b>0.60</b>
<b>Zikic [13]</b>	<b>0.70</b>	<b>0.71</b>	0.44	0.62	<b>0.62</b>
<b>Bauer [10]</b>	0.61	0.62	0.35	0.49	0.52
<b>Hamamci [14]</b>	0.56	0.73	<b>0.38</b>	<b>0.71</b>	<b>0.60</b>
<b>Geremia [15]</b>	0.56	0.58	0.29	0.20	0.41
<b>Zhao [11]</b>	-	-	-	-	0.33
<b>Subbanna [11]</b>	-	-	-	-	<b>0.61</b>
<b>Fernandez [11]</b>	-	-	-	-	0.49
<b>Menze[11]</b>	0.57	0.56	0.42	0.24	0.45
<b>Menze[11]</b>	0.70	0.71	0.49	0.23	0.54
<b>Riklin[11]</b>	0.61	0.59	0.36	0.32	0.52

## 4. CONCLUSION

We presented a brain tumor segmentation system from multi-spectral MRI images. The system is based on classification and uses a MKL-SVM algorithm. It allows to deal with multi-input data, to exploit the diversity and the complementarity of all used data and to automatically select the most informative features thanks to a sparsity constraint posed on kernel weights.

Our MKL-SVM algorithm is followed by a post-processing step : The tumor region resulting from our first learning is eroded and the MKL-SVM algorithm is applied on the eroded area. The final result is the fusion of the first and the second learning results.

Our system was tested on the real data provided by the challenge of Brats 2012. The results show good performances of our system.

It is important to note that our method is general and can be used to segment any object from images multi-sequence. In future works we would like to test different MKL implementation, to involve more diverse features and kernels and to compare on brain tumor datasets labelled with many classes.

## 5. REFERENCES

- [1] S. Bauer, R. Wiest, L.P. Nolte and M. Reyes. "A survey of mri-based medical image analysis for brain tumor studies". *Physics in Medicine and Biology* 2013;58(13):R97.
- [2] N. Gordillo, E. Montseny and P. Sobrevilla. "State of the art survey on {MRI} brain tumor segmentation. Magnetic Resonance Imaging ".2013;31(8):1426 - 1438.
- [3] E.A. El-Dahshan, H.M. Mohsen, K. Revett and A.M. Salem. "Computer-aided diagnosis of human brain tumor through MRI: A survey and a new algorithm". *Expert Syst Appl* 2014;41(11).
- [4] X.W. Chen and M. Wasikowski. Fast: "A roc-based feature selection metric for small samples and imbalanced data classification problems". *In: Proceedings of the 14th ACM SIGKDD International Conference on Knowledge Discovery and Data Mining. KDD '08*; New York, NY, USA: ACM. ISBN 978-1-60558-193-4; 2008, p. 124-132.
- [5] L. Wang . "Feature selection with kernel class separability". *Pattern Analysis and Machine Intelligence, IEEE Transactions on* 2008;30(9):1534- 1546.
- [6] G.R Lanckriet, N. Cristianini, P. Bartlett, L.E. Ghaoui and M.I Jordan. "Learning the kernel matrix with semidefinite programming". *The Journal of Machine Learning Research* 2004;5:27-72.
- [7] N. Zhang, S. Ruan, S. Lebonvallet, Q. Liao and Y. Zhu. "Kernel feature selection to fuse multi-spectral mri images for brain tumor segmentation". *Computer Vision and Image Understanding* 2011;115(2):256 - 269.
- [8] T. Ojala, M. Pietikainen and T. Maenpaa. "Multiresolution gray-scale and rotation invariant texture classification with local binary patterns". *Pattern Analysis and Machine Intelligence, IEEE Transactions on* 2002;24(7):971- 987.
- [9] A. Rakotomamonjy, F. Bach, S. Canu and Y. Grandvalet. "Simplemkl". *Journal of Machine Learning Research* 2008;9(11).
- [10] S. Bauer, L.P. Nolte and M. Reyes. "Fully automatic segmentation of brain tumor images using support vector machine classification in combination with hierarchical conditional random field regularization". *Medical Image Computing and Computer-Assisted Intervention- MICCAI 2011* :354-361.
- [11] B. Menze, A. Jakab, S. Bauer, M. Prastawa, M. Reye and K. Van Leem-put. "The Multimodal Brain Tumor Image Segmentation Benchmark (BRATS) ". Tech. Rep, 2012.
- [12] N. Boughattas, M. Berar, K. Hamrouni, an S. Ruan. "Brain tumor segmentation from multiple MRI sequences using multiple kernel learning ". *ICIP 2014*: 1887-1891.
- [13] Zikic, D., Glocker, B., Konukoglu, E., Criminisi, A., Demiralp, C., Shotton, J., et al. Decision forests for tissue-speci\_c segmentation of high-grade gliomas in multi-channel mr. *In: Medical Image Computing and Computer-Assisted Intervention{MICCAI 2012*. Springer Berlin Heidelberg; 2012, p. 369-376.
- [14] Hamamci, A., Kucuk, N., Karaman, K., Engin, K., Unal, G.. Tumor-cut: Segmentation of brain tumors on contrast enhanced mr images for radiosurgery applications. *Medical Imaging, IEEE Transactions on* 2012;31(3):790-804.
- [15] Geremia, E., Clatz, O., Menze, B., Konukoglu, E., Criminisi, A., Ayache, N.. Spatial decision forests for ms lesion segmentation in multi-channel magnetic resonance images. *NeuroImage* 2011;57(2):378-390.